

Article

Multi-Scale Coal Fire Detection Based on an Improved Active Contour Model from Landsat-8 Satellite and UAV Images

Yanyan Gao ¹, Ming Hao ^{1,*}, Yunjia Wang ¹, Libo Dang ² and Yuecheng Guo ³

¹ Jiangsu Key Laboratory of Resources and Environmental Information Engineering, China University of Mining and Technology, Xuzhou 221116, China; gaoyanyan@cumt.edu.cn (Y.G.); wyj4139@cumt.edu.cn (Y.W.)

² Geographic Information Branch, China Coal Aerial Remote Sensing Group Co., Ltd., Xi'an 710199, China; danglibo1987@163.com

³ Xinjiang Uygur Autonomous Region Coalfield Fire Fighting-Extinguishing Engineering Bureau, Urumqi 830063, China; guoyuecheng1216@163.com

* Correspondence: haoming@cumt.edu.cn

Abstract: Underground coal fires can increase surface temperature, cause surface cracks and collapse, and release poisonous and harmful gases, which significantly harm the ecological environment and humans. Traditional methods of extracting coal fires, such as global threshold, K-mean and active contour model, usually produce many false alarms. Therefore, this paper proposes an improved active contour model by introducing the distinguishing energies of coal fires and others into the traditional active contour model. Taking Urumqi, Xinjiang, China as the research area, coal fires are detected from Landsat-8 satellite and unmanned aerial vehicle (UAV) data. The results show that the proposed method can eliminate many false alarms compared with some traditional methods, and achieve detection of small-area coal fires by referring field survey data. More importantly, the results obtained from UAV data can help identify not only burning coal fires but also potential underground coal fires. This paper provides an efficient method for high-precision coal fire detection and strong technical support for reducing environmental pollution and coal energy use.

Keywords: coal fires; Landsat-8; UAV; multi-scale; active contour model



Citation: Gao, Y.; Hao, M.; Wang, Y.; Dang, L.; Guo, Y. Multi-Scale Coal Fire Detection Based on an Improved Active Contour Model from Landsat-8 Satellite and UAV Images. *ISPRS Int. J. Geo-Inf.* **2021**, *10*, 449. <https://doi.org/10.3390/ijgi10070449>

Academic Editors: Tao Cheng and Wolfgang Kainz

Received: 10 May 2021
Accepted: 29 June 2021
Published: 30 June 2021

Publisher's Note: MDPI stays neutral with regard to jurisdictional claims in published maps and institutional affiliations.



Copyright: © 2021 by the authors. Licensee MDPI, Basel, Switzerland. This article is an open access article distributed under the terms and conditions of the Creative Commons Attribution (CC BY) license (<https://creativecommons.org/licenses/by/4.0/>).

1. Introduction

Underground coal fires are usually caused by human factors, spontaneous combustion, forest fires, and natural hazards [1]. Coal fires are a common phenomenon in coalfields [2]. Underground coal fires exist in many parts of the world [3], such as India [4], the United States [5], and Australia [6]. In China, underground coal fires, mainly caused by human factors, are mostly distributed in Inner Mongolia Autonomous Region [7], Xinjiang Uygur Autonomous Region [8], Ningxia Hui Autonomous Region [9], and Shanxi Province [10]. Coal fires cause significant harm to the ecological environment and humans. Underground coal fires can release a lot of poisonous and harmful gases, such as SO₂, NO, CO, and CH₄ [11]. These gases can lead to an increase in harmful heavy metals, such as mercury, zinc, copper, lead, iron, and germanium. In addition, coal fires can also cause ground subsidence and cracks [12]. Coal fires have caused great harm to the ecological environment and human. Therefore, it is very important to prevent or delay coal fires [13,14]. Usually, a coal fire is extinguished by feeding different mixtures into the underground mine. Zhou et al. applied a three-phase foam, comprising silt, nitrogen, and water, to extinguish fires in the Baijigou Coal Mine of Ningxia Province in China [15]. Szurgacz et al. designed a new method to control coal fires by feeding an ash–water mixture or an ash–water mixture with carbon dioxide and achieved good results [16]. In the past, traditional geophysical and geochemical methods were used to detect coal fires. Although these methods have high detection accuracy, they are time consuming, labor intensive, inefficient, and dangerous [8]. Coal fire detection using a manual survey method is a challenging task, but this can be overcome with the help of remote sensing technology [17].

Thermal infrared remote sensing is the most common and effective method of monitoring wide coal fires [18]. Many kinds of remote sensing sensors capture the thermal infrared band, such as TM, ETM+, MODIS, ASTER, and AVHRR, which can be used to invert temperature information. The representative temperature inversion algorithms include the mono-window (MW) [19], single-channel [20], and split-window [21] algorithms. Gautam et al. used an intelligent wavelet transform method to detect underground coal fires based on NOAA–AVHRR images [22]. Wu et al. analyzed the factors affecting coal fire development in Xinjiang in terms of three different aspects [23]. Song et al. explored multidisciplinary investigations related to coal fires in China from 2004 to 2014, including fire detection, modeling, the assessment of environmental and human health impacts, and fire-fighting engineering [24]. Huo et al. studied the dynamics of coal fires in the Rujigou coalfield of Ningxia, from 2001 to 2007, using multi-temporal nighttime Landsat data [9]. Song et al. analyzed the impact of fire-fighting activities on the dynamic changes of the Wuda coalfield [25]. Xu et al. combined thermal infrared and time series InSAR technology to detect the Jiangjun Gobi fire area in Xinjiang [26]. Although these methods can detect large-area coal fires, they cannot effectively detect small area coal fires due to the low resolution of satellite thermal infrared data [9,27].

With the developments in the field of thermal infrared sensors and unmanned aerial vehicles (UAVs), it is now possible to map small coal fire areas with high accuracy, flexibility, and efficiency [28]. The equipment can solve the problem of the huge workload of data acquisition using handheld thermal infrared cameras. More importantly, UAV technology can acquire thermal infrared images with high spatial–temporal resolution [28]. Therefore, UAV thermal infrared data have been widely used to invert surface temperature. Leira et al. used a UAV with a thermal infrared camera to automatically detect, classify, and track sea objects [29]. Li et al. used UAV thermal infrared images to estimate annual CO₂ emissions in a coal fire area [30]. He et al. used UAV thermal infrared data to delineate the scopes and locations of a coal fire area [31]. Shao proposed a method of three-dimensional thermal surface imaging of coal fires based on UAV data [32].

The detection of coal fires using satellite or UAV data has some shortcomings. Satellite data cannot be used to detect small-area and potential coal fires due to low resolution [9,27]. In addition, studies usually use threshold or clustering methods to detect coal fires. These methods are simple and convenient, but they tend to extract many false temperature anomalies and need further analysis to determine real coal fires [9,27,28]. Therefore, this paper proposes an improved active contour model by introducing the distinguishing energies of coal fires and others into the traditional active contour model. It aims to eliminate false alarms caused by solar radiation, topographic undulation, types of surface features by enhancing differences between coal fires and others. The proposed method was implemented to satellite and UAV data simultaneously, which can realize coarse-to-fine coal fire detection by making full use of the advantages of satellite and UAV data.

The rest of this article is organized as follows: Section 2 gives a detailed description of the materials and the proposed method. Section 3 introduces the results and analysis of coal fire area extraction from satellite and UAV data. Section 4 further discusses the proposed method. Section 5 summarizes the main conclusions reached by this research.

2. Materials and Methods

2.1. Study Area

The study area is in Urumqi City, Xinjiang Uygur Autonomous Region, China, as shown in Figure 1. The central geographic coordinates are 43°56′ N and 87°48′ E. In this study, satellite data were acquired in the central part of Urumqi City. The main feature types include buildings, vegetation, and bare land. The range of UAV data was the Miqan coal fire area, in the southeast of Midong District, Urumqi City. In this area, the main cause of coal fires is that the coal seam is relatively shallow but quite thick [12,33]. The coal has a relatively high sulfur and phosphorus content [34]. The Miqan coal fire area is a typical case of coal fire disasters caused by abandoned coal kilns, the coal seam is mostly thicker

than 10 m, and the coal seam inclination is mostly 70° [12,33]. There are many cracks around the coal fire area; the fire is fierce and spreading rapidly. In addition, this area has heat storage conditions for coal seam combustion due to the large temperature difference and a dry environment. The previous mining of small coal mines and the inadequate technology of fire extinguishing are other causes of coal fires. This coal fire area is large, and the fire burns violently, causing significant wastage of coal resources and pollution. Large amounts of carbon dioxide, carbon monoxide, sulfur dioxide, smoke, and dust are emitted every year [34]. According to statistics, Xinjiang's annual coal loss is about 4.42 million tons, and the direct economic loss is approximately RMB 1 billion yuan [34]. Therefore, it is of great significance to develop methods for detecting underground coal fires.

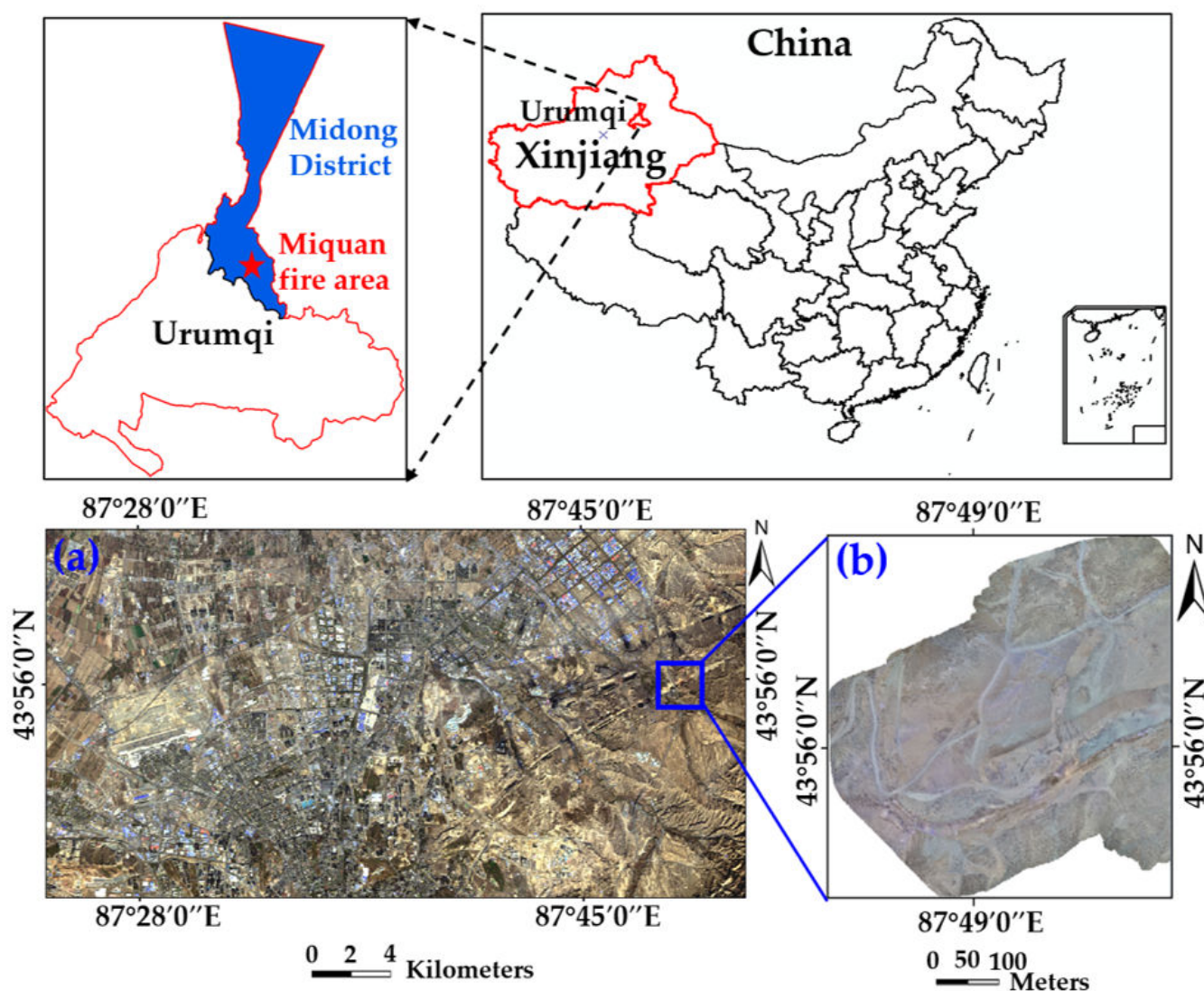


Figure 1. Location of the study area: (a) Landsat-8 image range and (b) UAV range.

2.2. Experimental Data

2.2.1. Satellite Data

In this study, the Landsat-8 image acquired on November 1, 2019, was used to calculate the land surface temperature (LST) and detect coal fire. The range of the image is shown in Figure 1a. The Landsat-8 satellite carries the Operational Land Imager (OLI) and the Thermal Infrared Sensor (TIRS). The spatial resolution of the multispectral and panchromatic bands is 30 and 15 m, respectively. The spatial resolution of the thermal infrared band is 100 m but resampled to 30 m in the delivered data products [35]. The

Landsat-8 satellite can achieve global coverage every 16 days and can be used to obtain the surface temperature across a wide range.

2.2.2. UAV Data

On 6 November 2019, the DJI M210 UAV equipped with a Zenmuse XT2 thermal infrared camera was used to obtain images of the Miqan coal fire area. The Zenmuse XT2 thermal infrared camera has many advantages, such as stable flight control, automatic obstacle avoidance, fast tracking, and display of the highest and lowest temperatures in an area. It is equipped with an FLIR long-wave infrared uncooled thermal imaging camera and a visible light camera. Therefore, it can simultaneously obtain thermal infrared and visible images. It also supports the fusion display of two images to provide more detailed information. For example, visible light and thermal infrared images, synchronously acquired by the UAV at $43^{\circ}56'5.10''$ N and $87^{\circ}48'56.54''$ E, are shown in Figure 2a,b, respectively. This research obtained a visual orthophoto and a thermal infrared image with a spatial resolution of 2.54 and 8.65 cm of the study area, respectively.

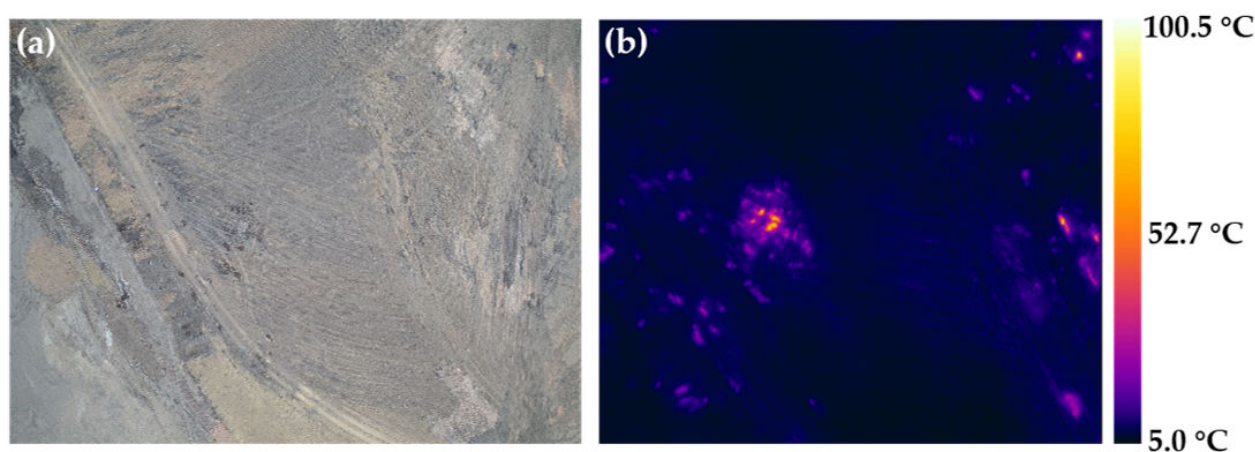


Figure 2. Visible and thermal infrared images synchronously acquired by a UAV: (a) visible image and (b) thermal infrared image.

2.3. Methods

This study proposes a coarse-to-fine coal fire detection method. The proposed method mainly consists of three steps. First, we invert the LST of the satellite image with the MW algorithm. The temperature information from the UAV data is obtained by stitching thermal infrared images with PIX4D mapper Version 4.5.2 software. Second, we calculate the average temperatures of the coal fires and others with the fuzzy C-means (FCM) algorithm and introduce the energies of these two parts into the traditional active contour model. Third, we extract coal fire areas from satellite and UAV data using the improved active contour model and verify the reliability of the results using a field survey. This procedure is graphically presented in the flowchart in Figure 3.

2.3.1. LST Inversion

Before temperature inversion, the Landsat-8 image needs to be pre-processed, which mainly includes radiometric calibration, atmospheric correction, image cropping, and NDVI calculation. Radiometric calibration and atmospheric correction are mainly used to eliminate or correct the image distortion caused by radiation errors. After pre-processing, temperature information can be further obtained and used to detect coal fires.

The MW algorithm was used to invert the LST in this study. The MW algorithm was proposed by Qin et al. [36] in 2001 and is a surface temperature inversion algorithm with only one thermal infrared band for TM data. It is a simple and feasible algorithm that only requires three parameters: emissivity, transmittance, and average atmospheric temperature [36,37]. The MW algorithm can also be applied to band 10 of the Landsat-8

image to invert the surface temperature [37]. The inversion equation of the MW algorithm is as follows:

$$T_S = \{a(1 - C - D) + [b(1 - C - D) + C + D]T_{\text{sensor}} - DT_a\} / C, \quad (1)$$

where T_S represents the surface temperature after inversion, and its unit is K; T_{sensor} represents the brightness temperature on the sensor (K); T_a represents the average temperature of the atmosphere (K); and a and b are constants. During the derivation of the temperature inversion equation, the relationship between the intermediate parameter L and the temperature T was close to linear. Therefore, in $L = a + bT$, when the temperature was 0~70 °C, the coefficients a and b were approximated as $a = -67.355351$ and $b = 0.458606$, with a relative estimate error $REE = 0.32\%$, correlation $R^2 = 0.9994$, T -test $T_{\text{test}} = 162.5$, and F-test $F_{\text{test}} = 108,328.6$. Both T -test and F-test were statistically significant at $\alpha = 0.001$, indicating that the approximate values of a and b were very successful [36]. C and D are intermediate variables, and their calculation equations are as follows:

$$\begin{cases} C = \varepsilon\tau \\ D = (1 - \tau)[1 + (1 - \varepsilon)\tau] \end{cases} \quad (2)$$

where ε represents the land surface emissivity (LSE). First, the vegetation coverage was calculated using the NDVI, and then the LSE was then further calculated through vegetation coverage [38]. τ represents atmospheric transmittance, which can be obtained directly by entering the latitude, longitude, and imaging time of the image on the NASA website.

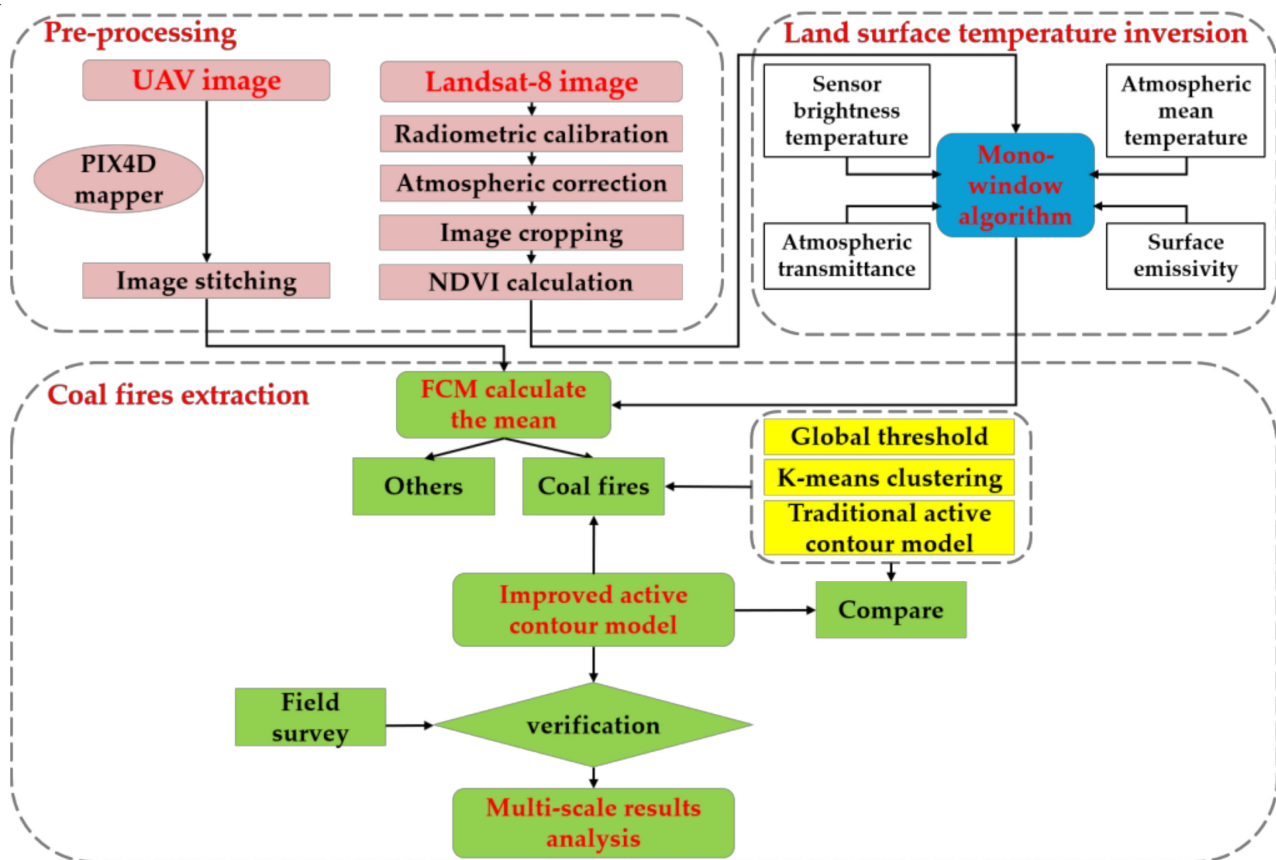


Figure 3. Flow chart of the coarse-to-fine coal fire detection method.

2.3.2. FCM Algorithm

During coal fire detection, it was necessary to divide the temperature image obtained by the MW algorithm into coal fires and others. The average temperatures of coal fires and others were obtained using the FCM algorithm. The FCM algorithm was first proposed by Dunn [39] and then popularized by Bezdek et al. [40]. It provides the membership degree of each sample point to all cluster centers by optimizing the objective function. Then, it determines the category of sample points and achieves automatic classification of sample data. The objective function of the FCM algorithm is shown in Equation (3).

$$J_m = \sum_{i=1}^N \sum_{j=1}^C \mu_{ij}^m \|x_i - c_j\|^2, \quad (3)$$

$$\mu_{ij} = \frac{1}{\sum_{k=1}^C \left(\frac{\|x_i - c_j\|}{\|x_i - c_k\|} \right)^{\frac{2}{m-1}}}, \quad c_j = \frac{\sum_{i=1}^N \mu_{ij}^m x_i}{\sum_{i=1}^N \mu_{ij}^m}, \quad (4)$$

where N represents the number of samples, C represents the number of clusters, $\{c_1, c_2, \dots, c_C\}$ represents the cluster center point set, m indicates the degree of fuzziness (usually, $m = 2$), and μ_{ij} represents the membership degree of the sample x_i belonging to the j -th category.

The temperature image was divided into coal fires and others through continuous iteration. If the sample was closer to the centroid, the membership was higher, else the membership was lower. The iteration stopped when the membership reached a relatively stable state. Based on the above FCM algorithm, the temperature image of the study area was divided into high-temperature coal fires and others, and the average temperatures of the two parts were obtained, which provided the initial values of input parameters for the next step.

2.3.3. Improved Active Contour Model

The Chan–Vese (CV) model was proposed by Chan and Vese in 2001 [41]. It is a typical regional active contour model, with a function expression, as given in Equation (5). Although the CV model can adapt well to topological changes in the evolution curve, it is sensitive to the initialization contour, and different initialization contours lead to different segmentation results [42]. In addition, the CV model has a poor effect on image segmentation, with an uneven grayscale [42]. This paper improved the CV model so it could be better applied to the field of coal fire detection. The distinguishing energies of coal fires and others were added to the traditional CV model based on the mean values obtained by the FCM algorithm. The improved active contour model is shown in Equation (6).

$$E(C) = \mu \text{Length}(C) + \nu \text{Area}(\text{In}(C)) + \lambda_1 \int_{\text{in}(C)} |I(x, y) - c_1|^2 dx dy + \lambda_2 \int_{\text{out}(C)} |I(x, y) - c_2|^2 dx dy \quad (5)$$

$$E(C) = \mu \text{Length}(C) + \nu \text{Area}(\text{In}(C)) + \lambda_1 \int_{\text{in}(C)} |I(x, y) - c_1|^2 dx dy + \lambda_2 \int_{\text{out}(C)} |I(x, y) - c_2|^2 dx dy + \int_{\text{in}(C)} |I(x, y) - c_3|^2 dx dy + \int_{\text{out}(C)} |I(x, y) - c_4|^2 dx dy \quad (6)$$

where $\text{Length}(C)$ represents the length of curve C , μ represents the length parameter, $\text{Area}(\text{In}(C))$ represents the area inside curve C , ν represents the area parameter, $I(x, y)$ represents the grayscale of any pixel in an image, c_1 represents the average temperature inside curve C , and c_2 represents the average temperature outside curve C . c_3 and c_4 , respectively, represent the average temperatures of high-temperature coal fires and others calculated by the FCM algorithm; λ_1 and λ_2 are constants; and $\lambda_1 > 0$, $\lambda_2 > 0$. Generally, $\lambda_1 = \lambda_2 = 1$, $\nu = 0$.

In this experiment, $\lambda_1 = \lambda_2 = 1$, $\nu = 0$. The level set method proposed by Osher and Sethian [43] was used to solve the function. C is the contour evolution curve, and the level set function φ was used to replace curve C in Equation (6). The above formula can be rewritten as Equation (7).

$$E(\varphi) = \mu E_1 + E_2 + E_3 + E_4 + E_5$$

$$\begin{cases} E_1 = \text{Length}(\varphi = 0) = \int_{\Omega} |\nabla H(\varphi)| dx dy = \int_{\Omega} \delta(\varphi) |\nabla \varphi| dx dy \\ E_2 = \int_{\Omega} |I(x, y) - c_1|_2 H(\varphi) dx dy \\ E_3 = \int_{\Omega} |I(x, y) - c_2|_2 (1 - H(\varphi)) dx dy \\ E_4 = \int_{\Omega} |I(x, y) - c_3|_2 H(\varphi) dx dy \\ E_5 = \int_{\Omega} |I(x, y) - c_4|_2 (1 - H(\varphi)) dx dy \end{cases} \quad (7)$$

$$H_{\varepsilon}(\varphi) = \begin{cases} 1 & \varphi > \varepsilon \\ 0 & \varphi < -\varepsilon \\ \frac{1}{2}(1 + \frac{2}{\pi} \arctan(\frac{\varphi}{\varepsilon})) & |\varphi| \leq \varepsilon \end{cases}, \quad \delta_{\varepsilon}(\varphi) = \begin{cases} 0 & |\varphi| > \varepsilon \\ \frac{1}{\pi} \frac{\varepsilon}{\varepsilon^2 + \varphi^2} & |\varphi| \leq \varepsilon \end{cases}, \quad (8)$$

where Ω represents an entire image area; $H_{\varepsilon}(\varphi)$ and $\delta_{\varepsilon}(\varphi)$ are normalized functions of Heaviside and Dirac, respectively; and ε is a small positive number.

The coal fire was detected by iterating continuously. The iteration termination condition of the active contour model includes two aspects: one is to manually set the number of iterations to different iteration times according to different images and research purposes [44,45]; the other is that the iteration stops when the level set function has converged [46,47]. In this paper, the maximum number of iterations was set to 500, and the algorithm continuously iterated until the level set function converged. The improved model can detect coal fires without clear boundaries and automatically change the topological structure. It can also achieve better segmentation without the initial contour. Therefore, the method discussed in this paper can be better applied to the monitoring of coal fires.

3. Results and Analysis

3.1. Results and Analysis Based on Satellite Data

The temperature inversion based on the satellite image using the MW algorithm ranged from 3.1 °C to 31.8 °C, the average temperature was 14.9 °C, and the standard deviation was 2.3 °C, as shown in Figure 4. The high-temperature areas were mainly distributed in the east of the study area. The weather in Urumqi City on 1 November 2019, was sunny, and the temperature ranged from 6 °C to 16 °C. Therefore, the temperature information obtained by the MW algorithm is reliable.

During combustion, the underground coal seam transfers heat to the ground in the form of thermal radiation. Then, a high-temperature environment is formed on the surface and in the air, called a temperature anomaly. Therefore, the temperature near the coal seam is higher than that of the surrounding ground. The first step in detecting coal fires was to find temperature anomalies and then verify them using a field survey. The average temperatures of coal fires and others calculated by the FCM algorithm were 16.8269 °C and 13.2820 °C, respectively. The improved active contour model was used to find temperature anomalies, which iterated 152 times and took 41.04 s. Figure 5a,b show the contour of temperature anomalies detected after 20 and 152 iterations, respectively. These iterative processes show the evolution of the detected temperature anomalies, and the finally extracted results of temperature anomalies are shown in the red area in Figure 5c.

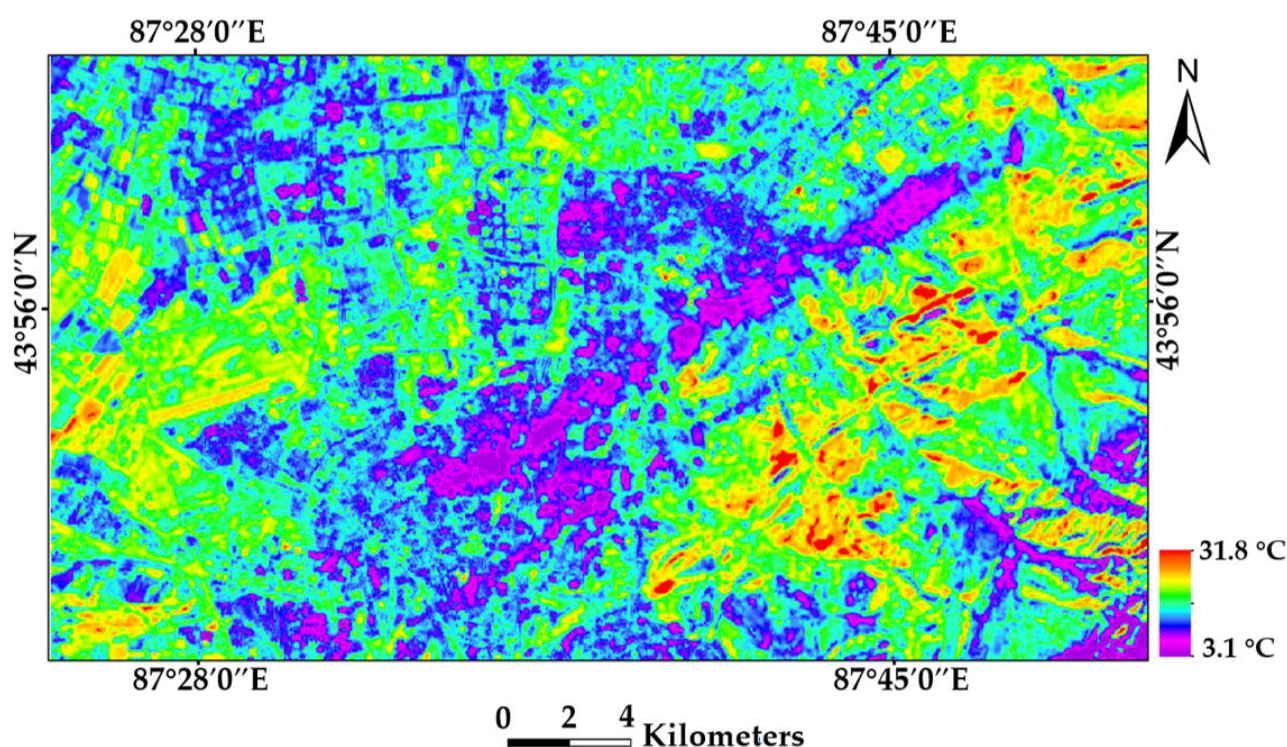


Figure 4. Result of LST inversion based on a Landsat-8 image.

The extracted results were validated using a field survey. The field conditions of the six areas are shown in Figure 6a–f. First, a large amount of smoke can be clearly seen in areas 4 and 5. There were burned rocks and gravel in areas 1, 3, and 6; mirabilite in areas 1, 3, 4, and 5; and sulfur in areas 1 and 5. These phenomena were caused by coal fires. Coal fires release a lot of toxic and harmful gases and dust particles during combustion, and the most important emissions are particulate matter, sulfur dioxide, nitrogen dioxide, and heavy metals [48]. Therefore, some particulate matter, such as sulfur, will appear on the surface after a series of chemical reactions. In addition, there was a crack in area 1, and the temperature was 70.7 °C, which provided oxygen for coal fires. In general, the temperature anomaly was caused by coal fires, and the improved active contour model has higher accuracy in coal fire detection.

Some traditional temperature anomaly detection methods, such as the global threshold [9], K-means clustering [43], and traditional active contour model [49], were also used to validate the effectiveness of the improved active contour model, and the results are shown in Figure 7. The global threshold was 19.5 °C (mean + 2 × standard deviation). The traditional active contour model iterated 13 times and took 6.1 s. However, there were many false alarms. For example, the temperature anomalies in areas I, II, and III were located on bare land, buildings, and the sunny side of mountains, respectively. In addition, the results of K-means clustering and the traditional active contour model were similar, and the range of temperature anomalies was relatively large. These false temperature anomalies were caused by solar radiation, topographic undulation, types of surface features, etc. Compared with these traditional methods, the improved active contour model achieved better results and eliminated many false alarms. This method can greatly reduce the workload of field verification and is of great significance in the field of coal fire detection.

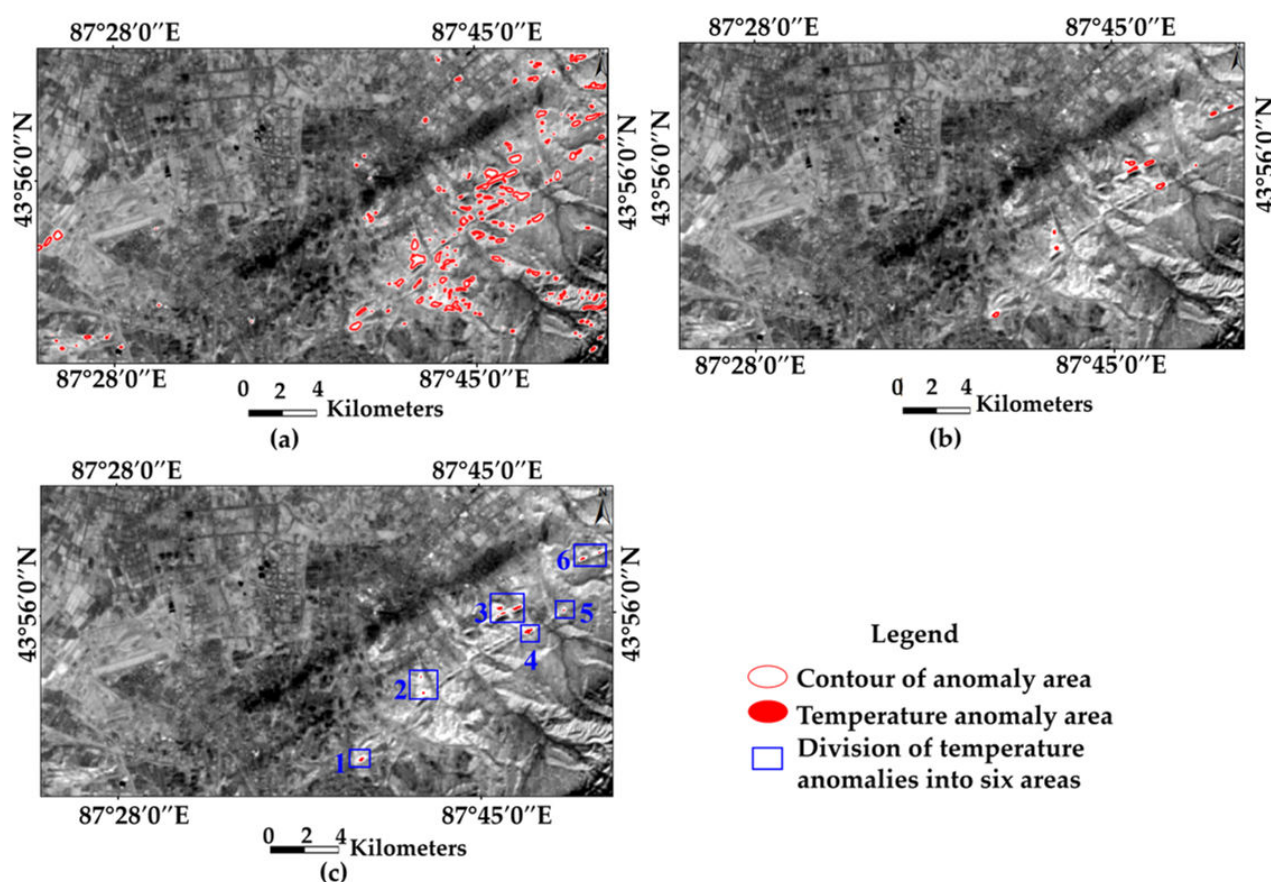


Figure 5. Process of detecting temperature anomalies using satellite data: (a) 20 iterations, (b) 152 iterations, and (c) final temperature anomaly results.

3.2. Results and Analysis Based on UAV Data

The temperature result of UAV data in the study area was obtained using PIX4D mapper version 4.5.2 (Figure 8), and the temperature ranged from -3.7°C to 102.0°C . The range of the Miqan coal fire area collected by the UAV was in area 5 of the Landsat-8 image. This further validated the reliability of using the improved active contour model to detect temperature anomalies. Therefore, the improved active contour model was implemented to detect coal fires from the UAV thermal infrared image. The average temperatures of coal fires and others calculated by the FCM algorithm were 12.5°C and 4.2°C , respectively. The distinguishing energies of two parts were added to the traditional active contour model. The improved active contour model was used to detect coal fires, which iterated 48 times and took 472.3 s. Figure 9a,b show the contour of the coal fire area after 20 and 48 iterations, respectively. The coal fire area was continuously refined by iteration. In addition, according to the characteristics of coal fire combustion and development, coal fires were generally not isolated points. Therefore, the 3×3 median filter was used to eliminate sporadic points. The coal fire area finally extracted from UAV data is shown in Figure 9c.

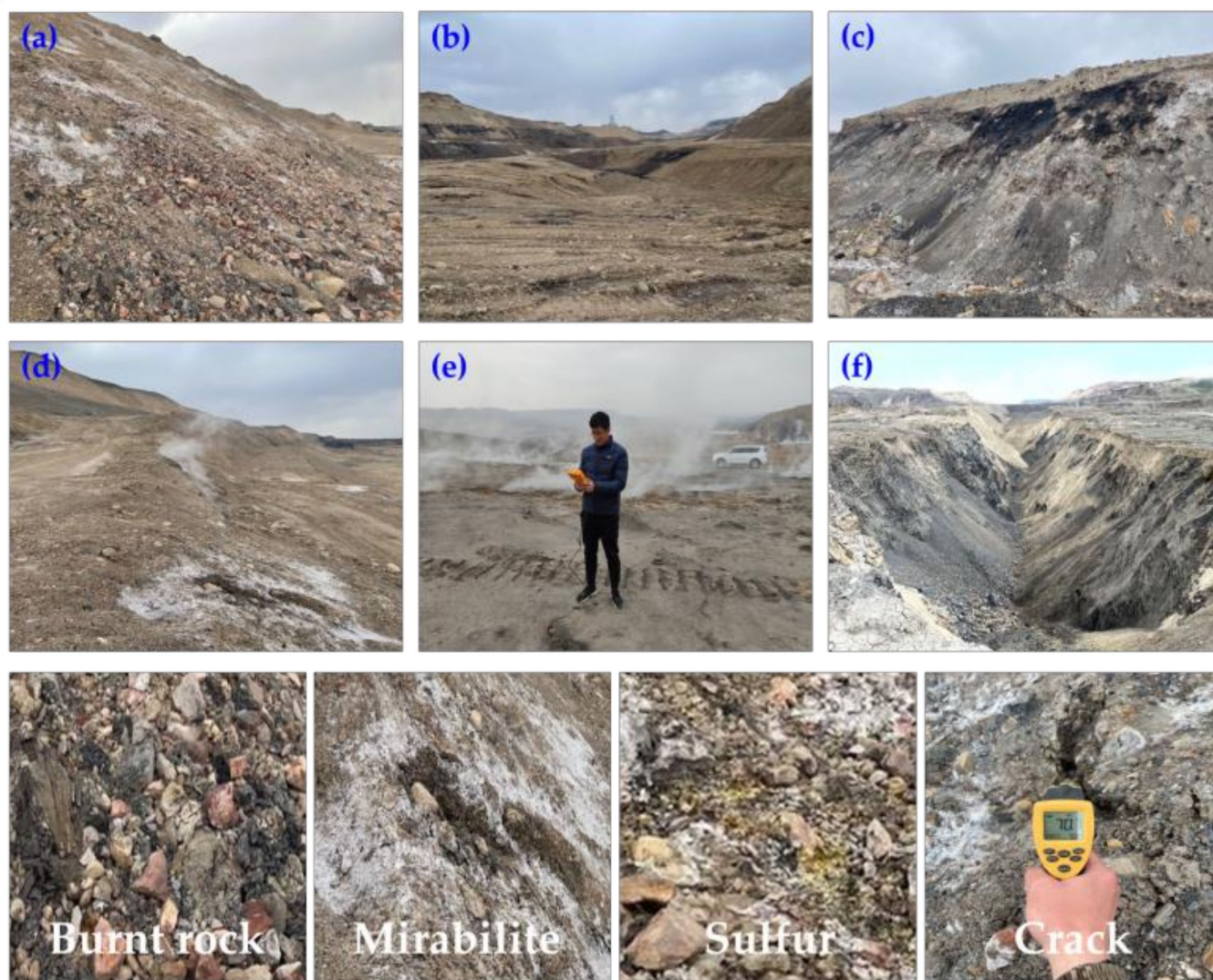


Figure 6. Field verification of satellite extraction results: areas (a) 1, (b) 2, (c) 3, (d) 4, (e) 5, and (f) 6.

The UAV data extraction result was validated using a field survey, and the corresponding relationship between them is shown in Figure 10. In areas 5-1, 5-2, and 5-3, there was a lot of thick smoke coming out of the ground. A large amount of sulfur can also be clearly seen in areas 5-1 and 5-3. These phenomena were caused by underground coal fires. However, there was no obvious smoke in areas 5-4 and 5-5 because the underground coal fires in these areas have been successfully extinguished. However, some coal fires have reignited over time. These areas that have reignited fires but no obvious burning phenomenon on the ground are called potential coal fire areas. In this study, both burning and potential coal fire areas could be extracted from UAV data using the improved active contour model. This is of great value for coalfield firefighting.

Figure 11 shows the points measured in the field using a DELIXI DECENTMT11350 infrared thermometer. These points were in or near coal fire areas, and all their temperatures were higher than 30 °C, sometimes even more than 70 °C. The differences between UAV and measured temperatures were below 2 °C, which showed that UAV temperatures can be used to accurately detect coal fires. In addition, to further compare the relationship between the ground measured temperatures and the corresponding temperatures in UAV images, linear regression was implemented. Figure 12 shows a strong positive correlation between the two kinds of temperatures, where R^2 was 0.9931 and the root-mean-square error (RMSE) was 1.5532 °C. The regression analysis result shows that the temperature

obtained by the UAV and the ground measured temperature have good consistency in the spatial dimension.

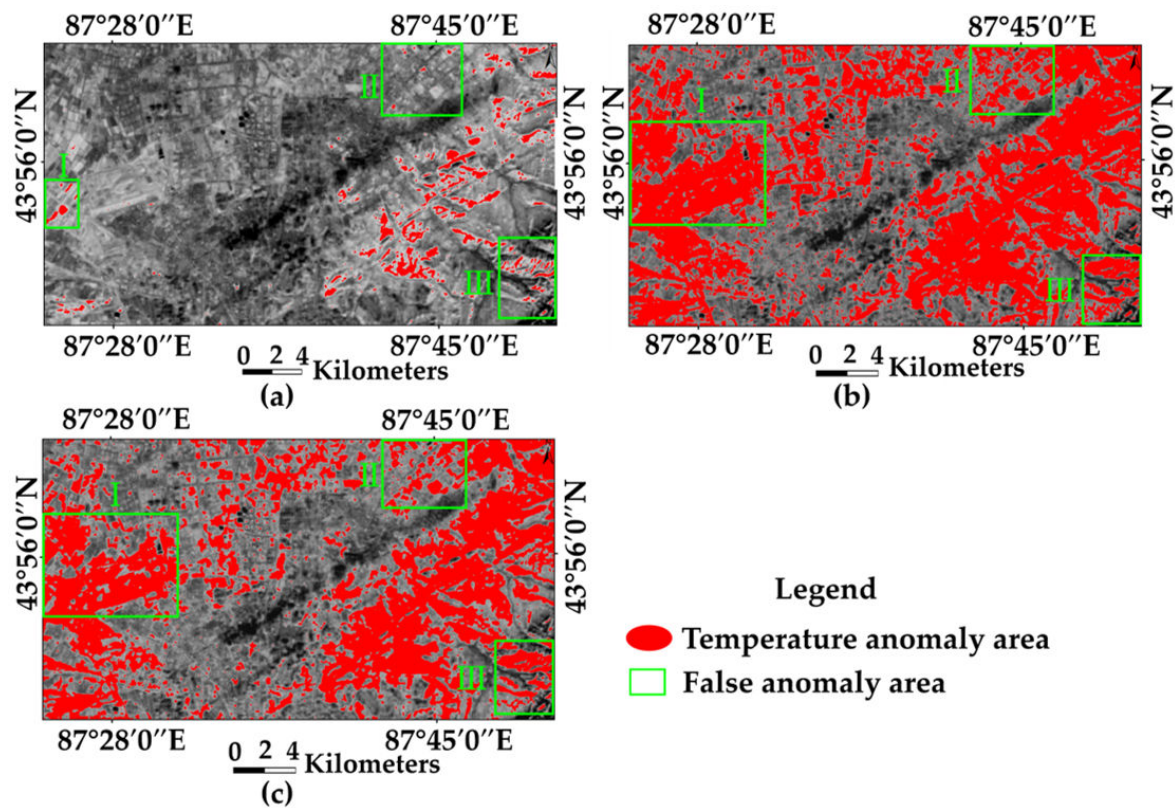


Figure 7. Temperature anomalies extracted by (a) global threshold, (b) K-means clustering, and (c) traditional active contour model.

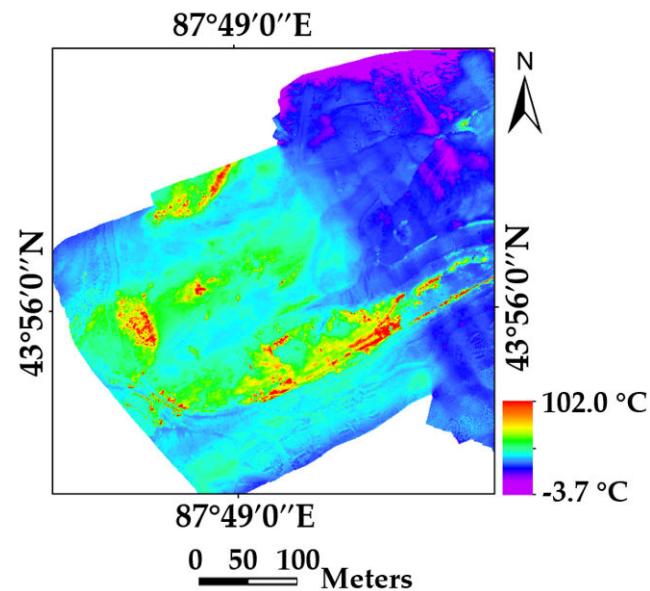


Figure 8. LST result based on UAV image.

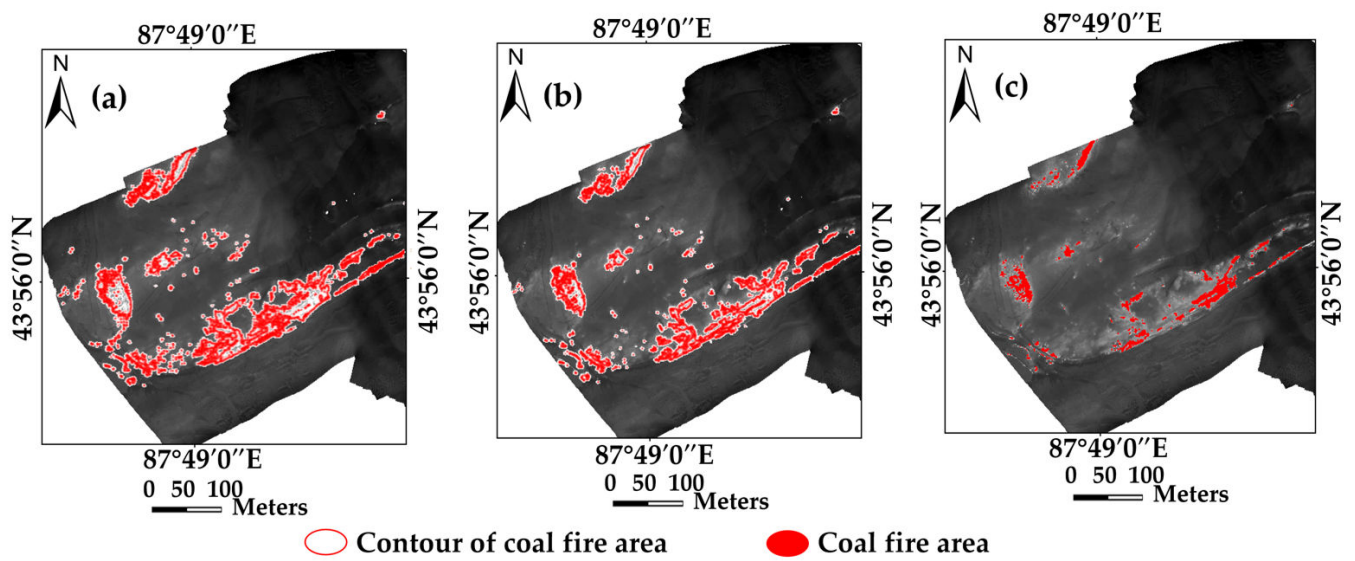


Figure 9. Process of extracting coal fire areas from UAV data: (a) 20 iterations, (b) 48 iterations, and (c) final coal fire results.

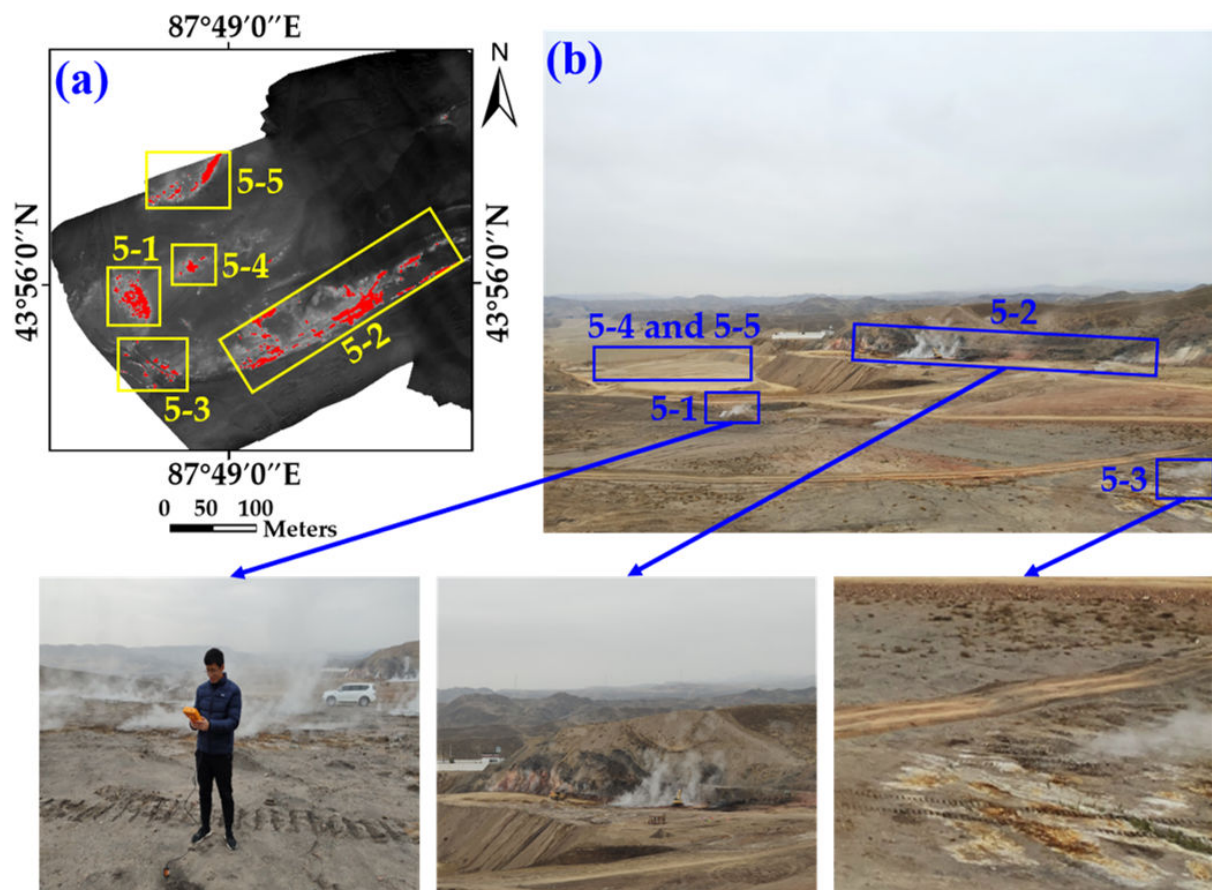


Figure 10. Field verification of UAV extraction result: (a) coal fire areas extracted from UAV data and (b) field survey.

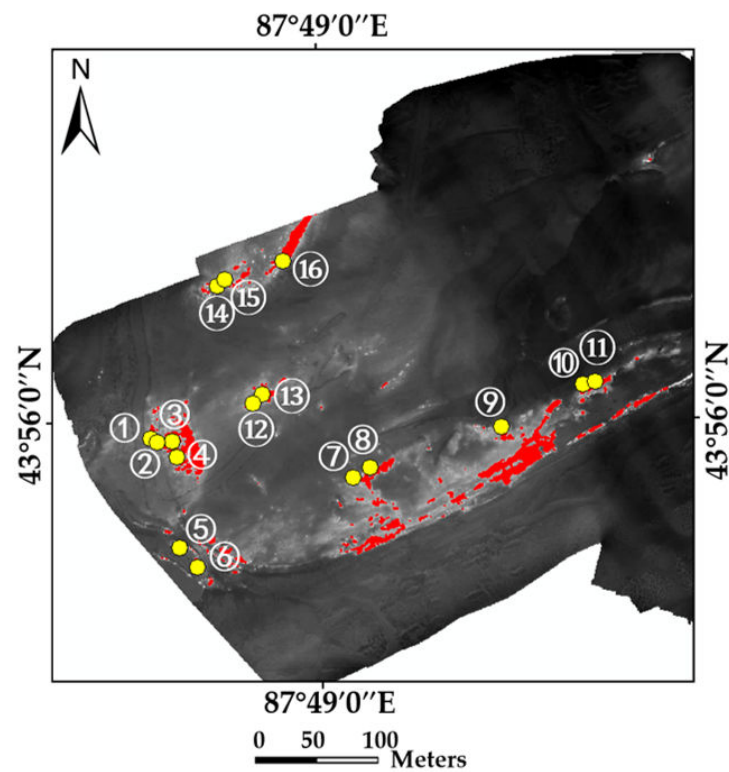


Figure 11. Location of data points measured in the field.

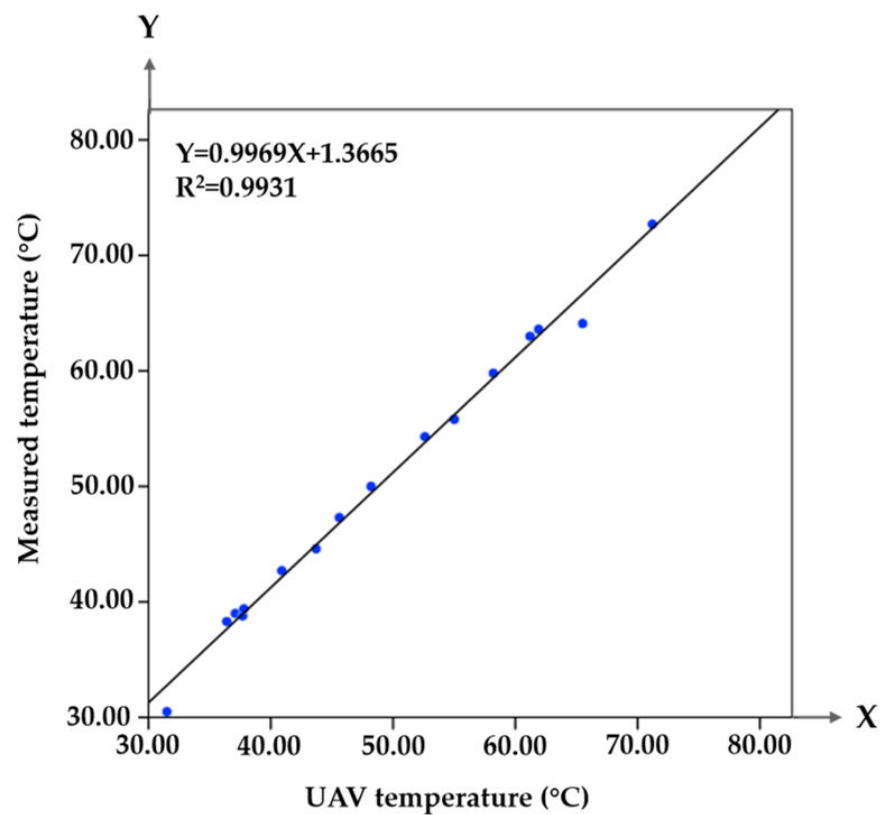


Figure 12. Relationship between UAV temperatures and ground measured temperatures.

4. Discussion

The large temperature difference and the dry environment in Urumqi City, Xinjiang, provide favorable conditions for coal fires. Coal fires increase surface temperature and

decrease humidity, so TIRS data are usually used to detect underground coal fires [18,35]. Many studies on coal fires validate the detection reliability by comparing the overlap rate between the temperature anomalies extracted from satellite data and the boundary map of a coal mine [17,50]. In this study, the distinguishing energies of coal fires and others were introduced into the traditional active contour model and the improved active contour model was used to detect coal fires, which had not been previously considered. Compared with the global threshold, K-means, and traditional active contour model methods, the improved active contour model can eliminate many false alarms caused by solar radiation, topographic undulation, and surface features, as shown in Figures 5c and 7. The reliability of the proposed method was further validated using a field survey. The proposed method can greatly reduce the workload of field verification and is of great significance for coal fire detection.

For achieving high-precision detection of Xinjiang coal fire areas, an integration of satellite and UAV techniques was used. Landsat-8 satellite data have the advantages of large coverage, low cost, and easy access, but due to the low spatial resolution of the thermal infrared band [35], the data can be only used for preliminary detection of coal fires. However, some coal fires that have no obvious burning phenomenon on the ground may not be detected by satellite data with low resolution [9,27]. Therefore, high-resolution UAV thermal infrared data are needed for further refined detection. In addition, the UAV temperature has a good positive correlation with the temperature measured by the infrared thermometer for coal fire detection, as shown in Figure 12, which is consistent with previous research [28]. Therefore, the surface temperature obtained by a UAV infrared camera has higher accuracy, which can be used to detect small-area or potential coal fires.

Figure 13 shows the area of each range in the results detected by satellite and UAV data. The total area of temperature anomalies extracted from Landsat-8 satellite data was 45.25 hectares, of which area 5 was 1.33 hectares. The total area of coal fires extracted from UAV data was 0.43 hectares, which was 0.9 hectares less than the area of zone 5 in Landsat-8 satellite results. The coal fire areas extracted from satellite data are relatively large, but the high-resolution UAV thermal infrared data can more precisely detect some typical coal fire areas. More importantly, UAV technology can also detect potential coal fire areas. This paper applied the active contour model to the field of coal fire monitoring and provided a new technical method for coal fire detection. The results and analysis can provide a reference for decision makers to manage environmental pollution and save energy.

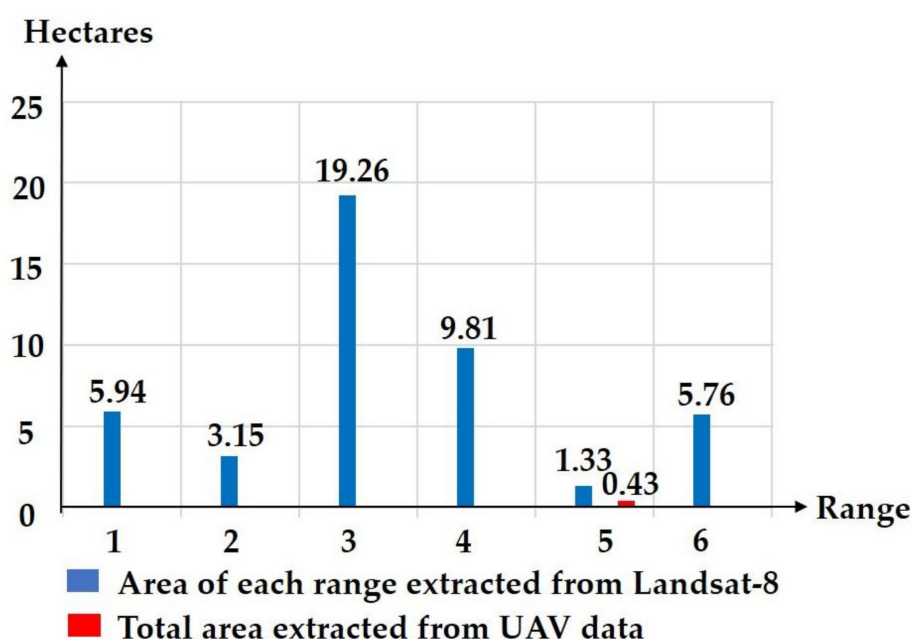


Figure 13. Area of each coal fire range extracted from satellite and UAV data.

This study had a few limitations. It is time consuming to extract coal fires from high-resolution data using the improved active contour model. In this paper, the size of UAV data was 5000×5000 pixels. The process of extracting coal fires from UAV data took 472.3 s. The collection of large amounts of UAV data is another limitation. Although the image resolution obtained by a UAV is relatively high, data collection is difficult and the cost of acquiring large-scale UAV data increases significantly [51,52]. Fernández-Guisuraga et al. used a UAV to collect data for post-fire monitoring in a 3000-hectare area. The overall procedure was time consuming and computationally demanding, taking 2 months to conduct and approximately 320 h for further data processing [53]. Therefore, it is recommended to first use satellite data for large-scale coal fire detection to preliminarily determine the range of coal fires. Then, according to the research purpose, high-resolution UAV data can be used to refine some target coal fire areas and obtain higher-precision results.

5. Conclusions

Traditional coal fire detection methods are time consuming, labor intensive, and inefficient, and using only single-satellite remote sensing data to detect coal fires can raise many false alarms and have low accuracy. Therefore, an improved active contour model was proposed for coal fire detection by simultaneously making full use of the advantages of satellite and UAV data, which realized a coarse-to-fine method of coal fire detection. The following conclusions are drawn:

- (1) Compared with the global threshold, K-means clustering, and traditional active contour model methods, the improved active contour model can provide better coal fire detection results. It eliminates false alarms caused by solar radiation, topographic undulation, surface features, etc. This method can greatly reduce the workload of field verification and improve the efficiency of coal fire detection.
- (2) Satellite data can be used for large-scale coal fire detection. These data can help in the preliminary detection of the range of a coal fire, which greatly reduces the blindness of firefighting work. However, due to their low resolution, the accuracy of detecting small-area and deep coal fires is limited.
- (3) High-resolution UAV data can be used to detect some target coal fire areas. The results based on UAV data extraction are validated using field surveys. There is good correlation between UAV results and field surveys. More importantly, UAV data can help detect extract both burning and potential coal fire areas.

Author Contributions: Conceptualization, Yanyan Gao, Ming Hao and Yunjia Wang; methodology, Yanyan Gao, Ming Hao and Yunjia Wang; investigation, Libo Dang and Yuecheng Guo; validation, Ming Hao, Yunjia Wang, Libo Dang and Yuecheng Guo; resources, Yanyan Gao; data curation, Yanyan Gao; formal analysis, Ming Hao; writing—original draft preparation, Yanyan Gao; writing—review and editing, Yanyan Gao, Ming Hao, Yunjia Wang, Libo Dang and Yuecheng Guo. All authors have read and agreed to the published version of the manuscript.

Funding: This work was supported by the Fundamental Research Funds for the Central Universities under Grant 2021YCPY0113 and a Project Funded by the Priority Academic Program Development of Jiangsu Higher Education Institutions.

Acknowledgments: The authors acknowledge and appreciate the support of the Fundamental Research Funds for the Central Universities under Grant 2021YCPY0113 and a Project Funded by the Priority Academic Program Development of Jiangsu Higher Education Institutions. In addition, the authors would like to thank each reviewer for their valuable comments, who have greatly improved the quality of the manuscript.

Conflicts of Interest: The authors declare no conflict of interest.

References

- Kuenzer, C.; Zhang, J.; Sun, Y.; Jia, Y.; Dech, S. Coal fires revisited: The Wuda coal field in the aftermath of extensive coal fire research and accelerating extinguishing activities. *Int. J. Coal Geol.* **2012**, *102*, 75–86. [\[CrossRef\]](#)
- Kruszewski, L.; Fabiańska, M.J.; Segit, T.; Kusy, D.; Motyliński, R.; Ciesielczuk, J.; Deput, E. Carbon nitrogen compounds, alcohols, mercaptans, monoterpenes, acetates, aldehydes, ketones, SF₆, PH₃, and other fire gases in coal-mining waste heaps of Upper Silesian Coal Basin (Poland)-are-investigation by means of in situ FTIR external database approach. *Sci. Total Environ.* **2020**, *698*, 1–16. [\[CrossRef\]](#)
- Oliveira, M.L.S.; Navarro, O.G.; Crissien, T.J.; Tutikian, B.F.; da Boit, K.; Teixeira, E.C.; Cabello, J.J. Coal emissions adverse human health effects associated with ultrafine/nano-particles role and resultant engineering controls. *Environ. Res.* **2017**, *158*, 450–455. [\[CrossRef\]](#) [\[PubMed\]](#)
- Roy, P.; Guha, A.; Kumar, K.V. An approach of surface coal fire detection from ASTER and Landsat-8 thermal data: Jharia coal field, India. *Int. J. Appl. Earth Obs. Geoinf.* **2015**, *39*, 120–127. [\[CrossRef\]](#)
- Engle, M.A.; Olea, R.A.; O’Keefe, J.M.K.; Hower, J.C.; Geboy, N.J. Direct estimation of diffuse gaseous emissions from coal fires: Current methods and future directions. *Int. J. Coal Geol.* **2013**, *112*, 164–172. [\[CrossRef\]](#)
- Ellyett, C.D.; Fleming, A.W. Thermal infrared imagery of The Burning Mountain coal fire. *Remote Sens. Environ.* **1974**, *3*, 79–86. [\[CrossRef\]](#)
- Zhang, J.; Kuenzer, C. Thermal surface characteristics of coal fires 1 results of in-situ measurements. *J. Appl. Geophys.* **2007**, *63*, 117–134. [\[CrossRef\]](#)
- Shao, Z.L.; Wang, D.M.; Wang, Y.M.; Zhong, X.X. Theory and application of magnetic and self-potential methods in the detection of the Heshituoluogai coal fire, China. *J. Appl. Geophys.* **2014**, *104*, 64–74. [\[CrossRef\]](#)
- Huo, H.Y.; Jiang, X.G.; Song, X.F.; Li, Z.L.; Ni, Z.Y.; Gao, C.X. Detection of Coal Fire Dynamics and Propagation Direction from Multi-Temporal Nighttime Landsat SWIR and TIR Data: A Case Study on the Rujigou Coalfield, Northwest (NW) China. *Remote Sens.* **2014**, *6*, 1234–1259. [\[CrossRef\]](#)
- Shao, Z.; Wang, D.; Wang, Y.; Zhong, X.; Tang, X.; Hu, X. Controlling coal fires using the three-phase foam and water mist techniques in the Anjialing Open Pit Mine, China. *Nat. Hazards* **2015**, *75*, 1833–1852. [\[CrossRef\]](#)
- Wang, G.; Cao, F.; Shan, B.; Meng, M.; Wang, W.; Sun, R.Y. Sources and Assessment of Mercury and Other Heavy Metal Contamination in Soils Surrounding the Wuda Underground Coal Fire Area, Inner Mongolia, China. *Bull. Environ. Contam. Toxicol.* **2019**, *103*, 828–833. [\[CrossRef\]](#)
- Liu, J.L.; Wang, Y.J.; Li, Y.; Dang, L.B.; Liu, X.X.; Zhao, H.F.; Yan, S.Y. Underground Coal Fires Identification and Monitoring Using Time-Series InSAR With Persistent and Distributed Scatterers: A Case Study of Miquan Coal Fire Zone in Xinjiang, China. *IEEE Access* **2019**, *7*, 164492–164506. [\[CrossRef\]](#)
- Tang, Y.; Wang, H. Experimental investigation on microstructure evolution and spontaneous combustion properties of secondary oxidation of lignite. *Process Saf. Environ. Prot.* **2019**, *124*, 143–150. [\[CrossRef\]](#)
- Zhang, Y.; Yang, C.; Li, Y.; Huang, Y.; Zhang, J.; Zhang, Y.; Li, Q. Ultrasonic extraction and oxidation characteristics of functional groups during coal spontaneous combustion. *Fuel* **2019**, *242*, 287–294. [\[CrossRef\]](#)
- Zhou, F.; Ren, W.X.; Wang, D.M.; Song, T.L. Application of three-phase foam to fight an extraordinarily serious coal mine fire. *Int. J. Coal Geol.* **2006**, *67*, 95–100. [\[CrossRef\]](#)
- Szurgacz, D.; Tutak, M.; Brodny, J.; Sobik, L.; Zhironkina, O. The Method of Combating Coal Spontaneous Combustion Hazard in Goafs—A Case Study. *Energies* **2020**, *13*, 4538. [\[CrossRef\]](#)
- Biswal, S.S.; Gorai, A.K. Change detection analysis in coverage area of coal fire from 2009 to 2019 in Jharia Coalfield using remote sensing data. *IJRS* **2020**, *41*, 9545–9564. [\[CrossRef\]](#)
- Syed, T.H.; Riyas, M.J.; Kuenzer, C. Remote sensing of coal fires in India: A review. *Earth-Sci. Rev.* **2018**, *187*, 338–355. [\[CrossRef\]](#)
- Jimenez-Munoz, J.C.; Sobrino, J.A.; Skokovic, D.; Mattar, C.; Cristobal, J. Land Surface Temperature Retrieval Methods from Landsat-8 Thermal Infrared Sensor Data. *IEEE Geosci. Remote Sens.* **2014**, *11*, 1840–1843. [\[CrossRef\]](#)
- Jimenez-Munoz, J.C.; Cristobal, J.; Sobrino, J.A.; Soria, G.; Ninyerola, M.; Pons, X. Revision of the Single-Channel Algorithm for Land Surface Temperature Retrieval from Landsat Thermal-Infrared Data. *IEEE Trans. Geosci. Remote Sens.* **2009**, *47*, 339–349. [\[CrossRef\]](#)
- Rozenstein, O.; Qin, Z.; Derimian, Y.; Karnieli, A. Derivation of Land Surface Temperature for Landsat-8 TIRS Using a Split Window Algorithm. *Sensors* **2014**, *14*, 5768–5780. [\[CrossRef\]](#)
- Gautam, A.; Gautam, R.S.; Saxena, N. An intelligent wavelet transform-based framework to detect subsurface fires with NOAA-AVHRR images. *IJRS* **2012**, *33*, 1276–1295. [\[CrossRef\]](#)
- Wu, J.J.; Liu, X.C. Risk assessment of underground coal fire development at regional scale. *Int. J. Coal Geol.* **2011**, *86*, 87–94. [\[CrossRef\]](#)
- Song, Z.Y.; Claudia, K. Coal fires in China over the last decade: A comprehensive review. *Int. J. Coal Geol.* **2014**, *72*–99. [\[CrossRef\]](#)
- Song, Z.Y.; Kuenzer, C.; Zhu, H.Q.; Zhang, Z.; Jia, Y.R.; Sun, Y.L.; Zhang, J.Z. Analysis of coal fire dynamics in the Wuda syncline impacted by fire-fighting activities based on in-situ observations and Landsat-8 remote sensing data. *Int. J. Coal Geol.* **2015**, *141*–142, 91–102. [\[CrossRef\]](#)
- Xu, Y.; Fan, H.D.; Dang, L.B. Monitoring coal seam fires in Xinjiang using comprehensive thermal infrared and time series InSAR detection. *IJRS* **2020**, *42*, 2220–2245. [\[CrossRef\]](#)

27. Jiang, W.; Jia, K.; Chen, Z.; Deng, Y.; Rao, P. Using spatiotemporal remote sensing data to assess the status and effectiveness of the underground coal fire suppression efforts during 2000–2015 in Wuda, China. *J. Clean. Prod.* **2017**, *142*, 565–577. [\[CrossRef\]](#)
28. Li, F.; Yang, W.; Liu, X.; Sun, G.; Liu, J. Using high-resolution UAV-borne thermal infrared imagery to detect coal fires in Majiliang mine, Datong coalfield, Northern China. *Remote Sens. Lett.* **2017**, *9*, 71–80. [\[CrossRef\]](#)
29. Leira, F.S.; Johansen, T.A.; Fossen, T.I. Automatic detection, classification and tracking of objects in the ocean surface from UAVs using a thermal camera. *IEEE Aerosp. Conf. Proc.* **2015**, *15*, 1–10. [\[CrossRef\]](#)
30. Li, F.; Qian, A.; Sun, G.; Wang, Q. Estimation of Annual CO₂ Emission from Coal Fires in Majiliang Mine, Datong, Northern China Using UAVs Thermal Infrared Remote Sensing Technology. *IEEE* **2018**, *18*, 1–4. [\[CrossRef\]](#)
31. He, X.; Yang, X.; Luo, Z.; Guan, T. Application of unmanned aerial vehicle (UAV) thermal infrared remote sensing to identify coal fires in the Huojitu coal mine in Shenmu city, China. *Sci. Rep.* **2020**, *10*, 13895. [\[CrossRef\]](#) [\[PubMed\]](#)
32. Shao, Z.; Li, Y.; Deng, R.; Wang, D.; Zhong, X. Three-dimensional-imaging thermal surfaces of coal fires based on UAV thermal infrared data. *IJRS* **2021**, *42*, 672–692. [\[CrossRef\]](#)
33. Liu, J.L.; Wang, Y.J.; Yan, S.Y.; Zhao, F.; Li, Y.; Dang, L.B.; Liu, X.X.; Shao, Y.Q.; Peng, B. Underground Coal Fire Detection and Monitoring Based on Landsat-8 and Sentinel-1 Data Sets in Miquan Fire Area, Xinjiang. *Remote Sens.* **2021**, *13*, 1141. [\[CrossRef\]](#)
34. Shao, Z.; Jia, X.; Zhong, X.; Wang, D.; Wei, J.; Wang, Y.; Chen, L. Detection, extinguishing, and monitoring of a coal fire in Xinjiang, China. *Environ. Sci. Pollut. Res.* **2018**, *25*, 26603–26616. [\[CrossRef\]](#) [\[PubMed\]](#)
35. Biswal, S.S.; Raval, S.; Gorai, A.K. Delineation and mapping of coal mine fire using remote sensing data—A review. *IJRS* **2019**, *40*, 6499–6529. [\[CrossRef\]](#)
36. Qin, Z.; Karnieli, A.; Berliner, P. A mono-window algorithm for retrieving land surface temperature from Landsat TM data and its application to the Israel-Egypt border region. *IJRS* **2001**, *18*, 456–466. [\[CrossRef\]](#)
37. Wang, L.; Lu, Y.; Yao, Y. Comparison of Three Algorithms for the Retrieval of Land Surface Temperature from Landsat 8 Images. *Sensors* **2019**, *19*, 5049. [\[CrossRef\]](#)
38. Qin, Z.; Li, W.; Gao, M.; Zhang, H. Estimation of Land Surface Emissivity for Landsat TM6 and its Application to Lingxian Region in North China. *SPIE* **2006**, 636618.1–636618.8. [\[CrossRef\]](#)
39. Dunn, J.C. A Fuzzy Relative of the ISODATA Process and Its Use in Detecting Compact Well-Separated Clusters. *Cybern. Syst.* **1973**, *3*, 32–57. [\[CrossRef\]](#)
40. Bezdek, J.C. A physical interpretation of fuzzy ISODATA. *IEEE Trans. Systems.* **1976**, SMC-6, 387–389. [\[CrossRef\]](#)
41. Chan, T.F.; Vese, L.A. Active contours without edges. *IEEE Trans. Image Process.* **2001**, *10*, 266–277. [\[CrossRef\]](#)
42. Wang, Z.; Liu, Y. Active contour model by combining edge and region information discrete dynamic systems. *Adv. Mech. Eng.* **2017**, *9*, 1–10. [\[CrossRef\]](#)
43. Osher, S.; Sethian, A.J. Fronts propagating with curvature-dependent speed: Algorithms based on Hamilton-Jacobi formulations. *J. Comput. Phys.* **1988**, *79*, 12–49. [\[CrossRef\]](#)
44. Biswas, S.; Hazra, R. Active contours driven by modified LoG energy term and optimized penalty term for image segmentation. *Inst. Eng. Technol.* **2020**, *14*, 3232–3242. [\[CrossRef\]](#)
45. Fang, J.; Liu, H.; Zhang, L.; Liu, J.; Liu, H. Region-edge-based active contours driven by hybrid and local fuzzy region-based energy for image segmentation. *Inf. Sci.* **2021**, *546*, 397–419. [\[CrossRef\]](#)
46. Yu, X.; Qi, Y.; Lu, Z.; Hu, N. Implicit Active Contours Driven by Local and Global Image Fitting Energy for Image Segmentation and Target Localization. *J. Sens.* **2013**, *1*, 1–8. [\[CrossRef\]](#)
47. Zhang, J.; Lu, Z.; Li, M. Active Contour-Based Method for Finger-Vein Image Segmentation. *IEEE* **2020**, *69*, 8656–8665. [\[CrossRef\]](#)
48. Pandey, B.; Agrawal, M.; Singh, S. Assessment of air pollution around coal mining area: Emphasizing on spatial distributions, seasonal variations and heavy metals, using cluster and principal component analysis. *Atmos. Pollut. Res.* **2014**, *5*, 79–86. [\[CrossRef\]](#)
49. Kass, A.W.D.T. Snakes: Active Contour Models. *J. Comput. Phys.* **1987**, *1*, 321–332. [\[CrossRef\]](#)
50. Li, F.; Liu, X.; Liu, J.; Wang, Q.; Qian, A. Remote Sensing Monitoring Research for Coal Fire in Wuda Coal Mining Using ASTER Thermal Infrared Images. In Proceedings of the 2016 4th International Workshop on Earth Observation and Remote Sensing Applications (EORSA), Guangzhou, China, 4–6 July 2016; Volume 193, pp. 47–51. [\[CrossRef\]](#)
51. Anderson, K.; Gaston, K. Lightweight unmanned aerial vehicles will revolutionize spatial ecology. *Front. Ecol. Env.* **2013**, *11*, 138–146. [\[CrossRef\]](#)
52. Pádua, L.; Guimarães, N.; Adão, T.; Sousa, A.; Peres, E.; Sousa, J. Effectiveness of Sentinel-2 in Multi-Temporal Post-Fire Monitoring When Compared with UAV Imagery. *Int. J. Geo-Inf.* **2020**, *9*, 225. [\[CrossRef\]](#)
53. Fernández-Guisuraga, J.; Sanz-Ablanedo, E.; Suárez-Seoane, S.; Calvo, L. Using Unmanned Aerial Vehicles in Postfire Vegetation Survey Campaigns through Large and Heterogeneous Areas: Opportunities and Challenges. *Sensors* **2018**, *18*, 586. [\[CrossRef\]](#)